Temperature-dependent interlayer coupling in Ni/Co perpendicular pseudo-spin-valve structures

S. M. Mohseni,[1,2,*] R. K. Dumas,[3] Y. Fang,[3] J. W. Lau,[4] S. R. Sani,[1,2] J. Persson,[2] and Johan Åkerman[1,2,3]

[1] *Materials Physics, School of Information and Communication Technology, KTH Royal Institute of Technology, Electrum 229, 164 40 Kista, Sweden*

[2] *NanOsc AB, Electrum 205, 164 40 Kista, Sweden*

[3] *Department of Physics, University of Gothenburg, 412 96 Gothenburg, Sweden*

[4] *Material Measurement Laboratory, National Institute of Standards and Technology, Gaithersburg, MD 20899, USA*

(Received 8 March 2011; revised manuscript received 27 October 2011; published 22 November 2011)

The temperature-dependent coupling mechanisms in perpendicular pseudo-spin valves based on the following structure, $[Ni/Co]_5/Cu(t_{Cu})/[Ni/Co]_2$, are investigated. Despite a thick ($t_{Cu} \geqslant 3$ nm) Cu spacer, room-temperature measurements reveal complete coupling of the $[Ni/Co]_5$ and $[Ni/Co]_2$ multilayers. This coupling can be attributed to strong long range magnetostatic stray fields that penetrate the spacer layer. This results in magnetic domain imprinting and vertically correlated domains throughout the reversal process. Surprisingly, when the temperature is reduced, a complete decoupling is observed. This somewhat counterintuitive result can be explained by a large difference in the $[Ni/Co]_5$ and $[Ni/Co]_2$ multilayer coercivities at reduced temperatures, which then impedes domain imprinting and promotes decoupling. Finally, the decoupling temperature is found to increase with spacer thickness.

DOI: 10.1103/PhysRevB.84.174432 PACS number(s): 75.75.−c, 75.70.Cn, 75.60.Ch, 75.47.−m

I. INTRODUCTION

Ni/Co multilayers (MLs) with perpendicular magnetic anisotropy (PMA), initially introduced almost 20 years ago,[1] have seen a recent upsurge in attention. This is primarily due to their advantages for a variety of spintronics devices, in particular those that rely on the spin-transfer torque (STT) effect,[2–10] e.g., STT-magnetic random access memory (STT-MRAM) and spin-torque oscillators (STOs). The utilization of materials with tilted and/or PMA in STT devices has shown, both theoretically and experimentally, faster switching, lower switching current, enhanced thermal stability, and low- to zero-field operation in STOs, than their fully in-plane magnetized counterparts.[2–16] Finally, the all-magnetic nature of Ni/Co MLs also allows for a unique combination of high spin polarization, high spin-torque efficiency, and easily tunable PMA.

Device architecture, whether it would be for STT-MRAM or STOs, is centered on a basic spin-valve or tunnel junction layer structure, where two ferromagnetic (FM) layers are separated by a metallic or insulating spacer, respectively. The electrical resistance of this trilayer is then proportional to the relative orientation of the magnetizations of the two FM layers, via the giant magnetoresistance (GMR) or tunneling magnetoresistance (TMR) effect. For proper operation, the FM layers should have distinct coercive, or switching, fields in order to provide the maximum possible change in GMR or TMR. This can be achieved by choosing, or engineering, layers with either a high (hard) or low (soft) anisotropy. However, interactions between FM layers must also be taken into account and minimized.[17–20] For example, manipulation of the soft layer has been shown to influence the magnetic configuration of the hard layer,[21–24] thus limiting functionality. There are a variety of different coupling mechanisms, each with a distinct physical mechanism and include (i) direct magnetic coupling through pinholes in the metallic or insulating spacer layer,[25] (ii) indirect exchange coupling via the Ruderman-Kittel-Kasuya-Yosida (RKKY) interaction,[26] (iii) orange peel (Néel) magnetostatic coupling[27,28] due to correlated roughness at both spacer interfaces, and (iv) magnetostatic coupling by stray fields.[28,29] Although magnetostatic coupling is negligible in a uniformly magnetized macroscopic sample, it may become significant when the FM layers are in a multidomain state or when the lateral size of the sample is reduced.[29] Magnetostatic coupling in systems with PMA plays a particularly important role.[28–32] For example, a progressive reduction in the remanent magnetization of a hard FM layer by repeated switching of a neighboring soft layer,[21] formation of mirrored and replicated domains in the hard and soft layers,[23,33] and lowering of the nucleation field,[34] have all been shown. As the stray fields emanate from the domains themselves, different domain sizes or shapes can lead to drastically different stray field amplitudes[29] and therefore interaction strengths.

In this paper, we investigate the coupling mechanisms in [Ni/Co] ML-based perpendicular pseudo-spin valves (PSVs). The interactions are studied both as a function of temperature and spacer thickness. All samples studied at room temperature show that reversal of the soft/hard layers proceeds by vertically correlated domains through the entire PSV film stack due to strong dipolar coupling through the Cu spacer. However, and somewhat surprisingly, for a fixed spacer thickness, a complete decoupling of the hard/soft [Ni/Co] MLs is found at reduced temperatures. This can be explained by considering the temperature dependence of the $[Ni/Co]_2$ and $[Ni/Co]_5$ ML coercivities, which in addition to showing an increase, also show a large relative difference at reduced temperatures. This impedes domain imprinting and hence promotes decoupling at reduced temperatures. Finally, the decoupling temperature is found to increase with spacer thickness.

II. EXPERIMENTAL

All film stacks were deposited at room temperature on thermally oxidized Si substrates using a magnetron sputtering system in a chamber with a base pressure better than 5×10^{-8} Torr. The Ar process gas pressure was maintained at 5 mTorr for all layers. The sputtering rate for Ni,

Co, and Cu were 0.42, 0.22, and 1.3 Å/s, respectively. The full PSVs have the following nominal layer structure: $[Ni(0.8)/Co(0.4)]_5/Cu(t_{Cu})/Co(0.4)/[Ni(0.8)/Co(0.4)]_2$, all thicknesses in nanometers and the Cu spacer thickness, t_{Cu}, is varied from 1–10 nm. In order to characterize the behavior of the individual MLs $[Ni(0.8)/Co(0.4)]_5/Cu(6)$ and $Cu(6)/[Ni(0.8)/Co(0.4)]_2$ (thickness in nanometers), stacks were also deposited and will simply be referred to as $[Ni/Co]_5$ and $[Ni/Co]_2$, respectively. In order to better reproduce the complete film structure of the full PSV, and as the PMA is sensitive to the thickness of Cu underlayer,[35] the individual films contain Cu underlayers and capping layers. Finally, all film stacks include 5 nm Ta seed and capping layers.

Structural and chemical analyses were performed by transmission electron microscopy (TEM) and electron energy-loss spectroscopy (EELS). Magnetic properties were characterized using a superconducting quantum interface device-vibrating sample magnetometer (SQUID-VSM), for variable temperature measurements, and an alternating gradient magnetometer (AGM) dedicated to room-temperature measurements. In addition to standard major hysteresis loop analysis, we employed the first-order reversal curve (FORC) technique, as described in prior publications.[36–38] To briefly summarize, after positive saturation the applied field, H, is reduced to a given reversal field, H_R. From this reversal field the magnetization is then measured back toward positive saturation, thereby tracing out a single FORC. This process is repeated for ever decreasing values of H_R, creating a family of FORCs, which fill the interior of the major hysteresis loop. From this family of FORCs, the FORC distribution is defined as the mixed second-order derivative of the magnetization $M(H,H_R)$, $\rho(H,H_R) \equiv -(1/2M_S)[\partial^2 M(H,H_R)/\partial H \partial H_R]$, which is typically plotted on a contour plot against (H, H_R) coordinates. Most important for the discussions here is that the FORC distribution provides a quantitative fingerprint of the reversal mechanism as it is only sensitive to the *irreversible* components to the switching. The temperature dependence of the current in-plane magnetoresistance (MR) of the samples was measured by Physical Properties Measurement System (PPMS) using a standard four-point measurement geometry with the applied field perpendicular to the film plane. Additionally, room temperature as-deposited domain images were acquired using magnetic force microscopy (MFM) in standard phase detection mode with low moment tips.

III. RESULTS

A high-resolution cross-sectional TEM image acquired at Si [110] of a PSV with a nominal Cu spacer layer of 6 nm is shown in Fig. 1(a). The grains tend to be columnar with a size of about 25 nm. The onset and termination of the Cu layer is often demarcated by stacking faults with the $[Ni/Co]_x$ neighbors. Additionally, upon careful analysis of the bright field images, we found that the thicknesses of our films are ~80% of the nominal values, which is further supported by EELS analysis. A 25-nm EELS line scan taken at 1-nm intervals was performed in the indicated area of Fig. 1(b). The histogram in Fig. 1(b) shows the background-subtracted Cu $L_{2,3}$ signal as a function of scan position. The Cu concentration clearly shows a peak corresponding to the Cu spacer. We use

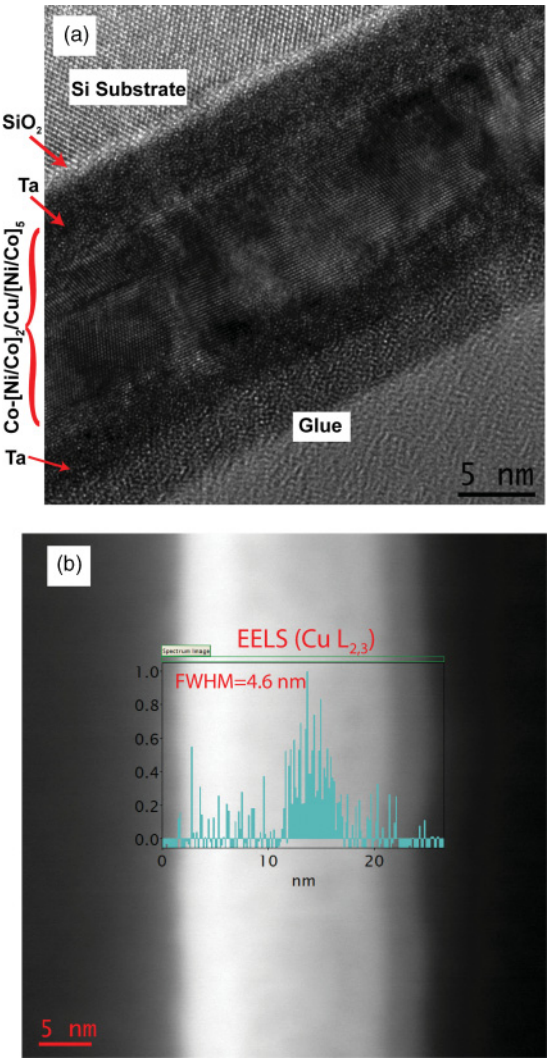

FIG. 1. (Color online) (a) High-resolution cross-sectional TEM image. (b) Scanning TEM image and an EELS line scan of the background subtracted Cu $L_{2,3}$ signal.

the full width at half maximum (FWHM) of 4.6 nm as a measure of the thickness of the Cu spacer and have scaled our nominal t_{Cu} values accordingly.

A. Room Temperature

The room-temperature hysteresis loops, measured with the applied field perpendicular to the film surface, of the isolated $[Ni/Co]_2$ (black squares) and $[Ni/Co]_5$ (red circles) MLs are shown in Fig. 2(a). The coercivities of the $[Ni/Co]_5$ and $[Ni/Co]_2$ MLs are 28 and 78 Oe, respectively. Although the $[Ni/Co]_5$ ML shows a reduced coercivity and remanence as compared to $[Ni/Co]_2$ ML, the easy axis of both MLs is indeed perpendicular to the film plane. The hysteresis loops measured with the applied field parallel to the film plane, inset of Fig. 2(a), not only reach saturation in a considerably larger field, but have a vanishing coercivity and remanence, consistent with an in-plane hard axis. The hysteresis loop (black squares) and the derivative of the descending branch (blue triangles) for the full PSV film stack with $t_{Cu} = 4.6$ nm, are shown in Fig. 2(b) for the field perpendicular to the film

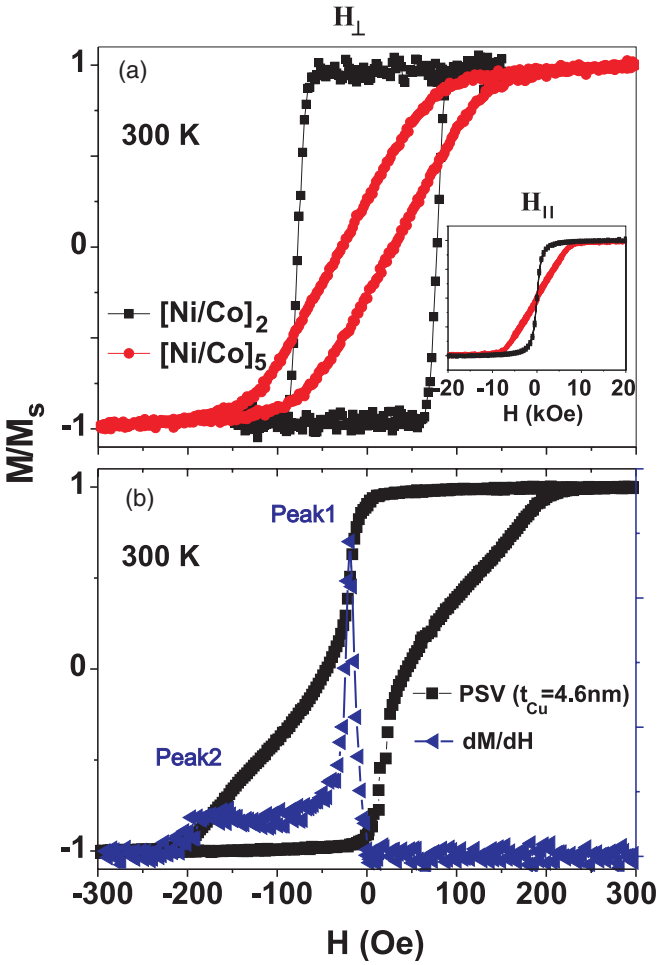

FIG. 2. (Color online) (a) Hysteresis loops of isolated $[Ni/Co]_2$ (black squares) and $[Ni/Co]_5$ (red [dark gray] circles) MLs measured with the applied field perpendicular to the film surface, inset shows measurements with the applied field parallel to the film surface. (b) Hysteresis loop of a PSV with $t_{Cu} = 4.6$ nm spacer layer (black squares) with the applied field perpendicular to the film surface along the derivative of the descending branch (blue [gray] triangles).

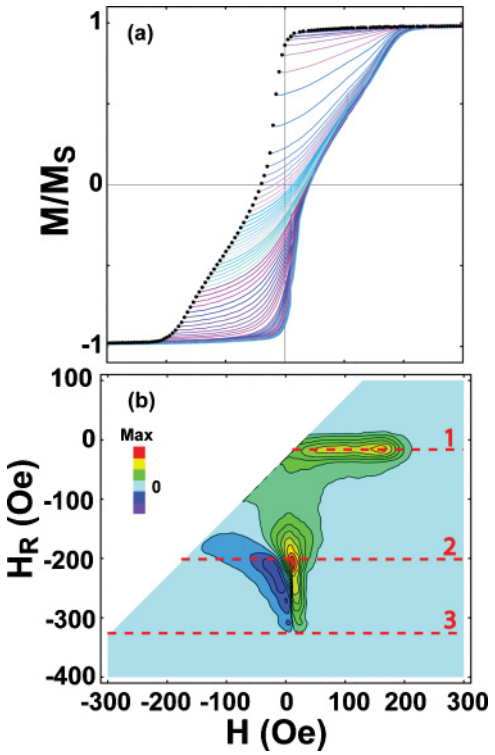

FIG. 3. (Color online) (a) Family of FORCs, whose starting points are represented by black dots, and (b) the corresponding FORC distribution plotted against (H, H_R) coordinates for the PSV with a $t_{Cu} = 4.6$ nm spacer. The dashed lines and numbers in (b) highlight features discussed in the text.

surface. Clearly, the behavior of the PSV is not a simple superposition of the individual MLs, shown in Fig. 2(a), and the overall shape is consistent with highly coupled reversal of the constituent MLs.[37–39] Additionally, while the loop derivative may suggest two switching fields, the locations of each peak (peak 1 = 19 Oe; peak 2 = 168 Oe) do not correspond to the switching fields of the individual MLs.

Further insight into the room-temperature reversal mechanisms are obtained by FORC measurements. The family of FORCs and corresponding FORC distribution are shown in Figs. 3(a) and 3(b), respectively. Inspection of the FORCs in Fig. 3(a) confirms a highly coupled reversal mechanism as the sharp reversal behavior of the $[Ni/Co]_2$ layer is completely absent from any of the FORCs. Furthermore, from a fingerprinting standpoint, the FORC distribution, Fig. 3(b), indicates reversal via vertically correlated domains, as previously reported in Co/Pt[38] and (Co/Pt)/Ru[37] ML systems. The FORC distribution, Fig. 3(b), is dominated by two primary irreversible features. The first feature, indicated with line scan 1 in Fig. 3(b), is a horizontal ridge, which corresponds to the initial rapid and irreversible drop in magnetization near $H_R = -20$ Oe and the nucleation of reverse domains. The second feature, highlighted with line scan 2 in Fig. 3(b), is a vertical negative/positive pair of peaks, $H_R = -200$ Oe, which indicates the onset of irreversible domain annihilation as negative saturation is approached. Two additional aspects of the FORC diagram are also worth commenting on. First, it can be seen that the area between line scans 1 and 2 is mostly featureless. This indicates the reversible domain expansion/contraction for these reversal fields. Finally, as is seen in Figs. 2(b) and 3(a), the major loop appears to reach negative saturation at $H = -220$ Oe. However, the FORC distribution indicates true saturation does not occur until much later, at $H_R = -330$ Oe, where the FORC distribution again becomes featureless, line scan 3 in Fig. 3(b). This interesting behavior is due to the large fields required to fully saturate microscopic bubble domains and hence reach true saturation.

Additional evidence for vertically correlated domains is provided by MFM. The MFM images for the as-deposited isolated $[Ni/Co]_2$ and $[Ni/Co]_5$ MLs are shown in Figs. 4(a) and 4(b), respectively. The domains in the $[Ni/Co]_2$ sample are sparsely scattered over a relatively large area (note the scale bar) as compared to the $[Ni/Co]_5$ sample, which shows a much finer domain structure, as expected due to its increased thickness.[29,40] Although the domain structure of the PSV, Fig. 4(c), is qualitatively similar to the $[Ni/Co]_5$ sample, the average domain size is noticeably smaller. It is important to note that in the PSV the $[Ni/Co]_5$ ML is buried below the

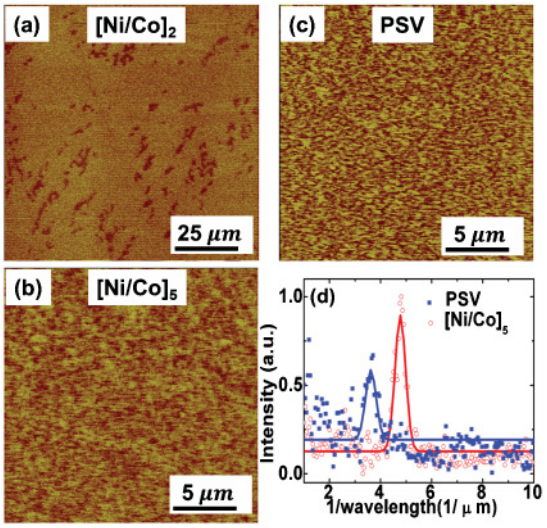

FIG. 4. (Color online) MFM images of (a) $[Ni/Co]_2$, (b) $[Ni/Co]_5$, and (c) PSV. (d) Power spectral densities obtained from the fast Fourier transformed MFM images with Gaussian fits.

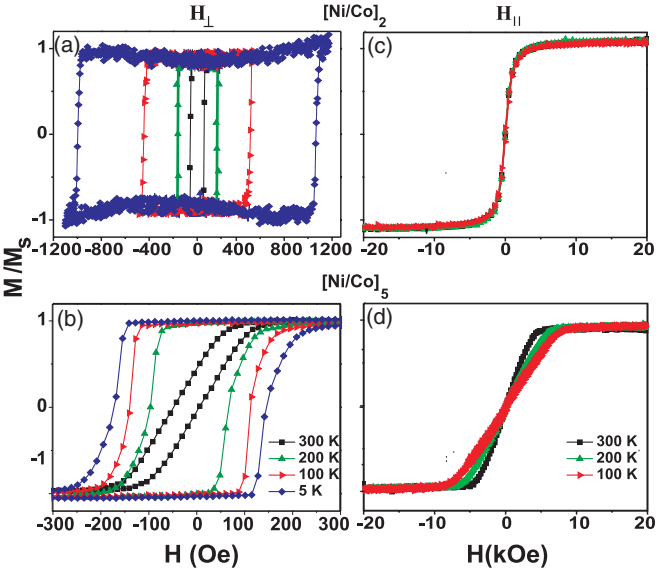

FIG. 5. (Color online) (left) Temperature-dependent perpendicular hysteresis loops for the isolated (a) $[Ni/Co]_2$ and (b) $[Ni/Co]_5$ MLs. (right) Temperature-dependent in-plane hysteresis loops for the isolated (c) $[Ni/Co]_2$ and (d) $[Ni/Co]_5$ MLs.

Cu spacer and $[Ni/Co]_2$ ML, and hence we are not simply imaging the $[Ni/Co]_5$ again. By taking a two-dimensional Fourier transform of the MFM images found in Figs. 4(b) and 4(c), a quantitative measure of the average domain periodicity can be obtained. The power spectral densities of the Fourier transforms are shown in Fig. 4(d), where Gaussian fits allow us to calculate the inverse of the average domain periodicity. The mean domain size, defined as half the domain periodicity, of the isolated $[Ni/Co]_5$ ML and PSV are 276 and 210 nm, respectively. In the fully coupled PSV, what matters most in determining the domain size is the total thickness of the two films, where in essence the film is now behaving as a Ni/Co ML with seven repeats and therefore has a reduced domain size as compared to the isolated $[Ni/Co]_5$ ML. In summary, at room temperature the major loop, FORCs, and MFM indicate that reversal proceeds by vertically correlated domains through both the $[Ni/Co]_5$ and $[Ni/Co]_2$ MLs mediated by the strong magnetostatic stray fields.

B. Temperature Dependence

Temperature-dependent hysteresis loops, measured with the applied field perpendicular to the film plane, for the isolated $[Ni/Co]_2$ and $[Ni/Co]_5$ MLs are shown in Figs. 5(a) and 5(b), respectively. The $[Ni/Co]_5$ ML shows a clear increase in squareness as the temperature is decreased below 200 K, consistent with prior reports on this material system.[41] Most notably, while both the isolated MLs show an increase in coercivity, Fig. 6(a), and saturation magnetization, Fig. 6(b), with reduced temperatures, the temperature dependence of the $[Ni/Co]_2$ ML is far more pronounced. Finally, we use the Sucksmith-Thompson method[42,43] in conjunction with the hard axis loops, shown in Figs. 5(c) and 5(d), to calculate the temperature dependence of the anisotropy K_u, Fig. 6(c).

The temperature-dependent hysteresis and MR loops for the PSV with $t_{Cu} = 4.6$ nm are shown in Figs. 7(a) and 7(b), respectively. Along with an overall broadening and increase in coercivity with reduced temperatures is a distinct decoupling of the $[Ni/Co]_2$ and $[Ni/Co]_5$ MLs. This is most clearly seen at 50 K, where the hysteresis loop clearly shows two distinct steps corresponding to independent reversal of the $[Ni/Co]_5$ ($H = \pm 170$ Oe) and $[Ni/Co]_2$ ($H = \pm 700$ Oe) MLs. As the majority of the magnetic signal is expected to be from the thicker $[Ni/Co]_5$ ML, its switching can be clearly distinguished from the thinner $[Ni/Co]_2$ ML. The derivative of the descending branch of the temperature-dependent hysteresis loops all show two distinct peaks, as seen in Fig. 2(b) at 300 K, and the absolute value of the location of these peaks is plotted as a function of temperature in Fig. 7(c). As the temperature is reduced from 300 K, both peaks 1 and 2 show a small increase as T = 175 K is approached. A splitting is observed as the location of peak 2 begins to show a pronounced increase as the temperature is decreased beyond 175 K. Accompanying the splitting of the derivative peaks is a sudden increase in the maximum MR, Fig. 7(d), which shows a pronounced increase for T < 175 K as the $[Ni/Co]_5$ and $[Ni/Co]_2$ MLs decouple at reduced temperatures.

IV. DISCUSSION

The behavior of the observed coupling mechanism, in particular its temperature dependence, is somewhat counterintuitive. Taking into account the thick spacer layer and complete decoupling at reduced temperatures, RKKY, direct exchange coupling through pinholes, and Néel coupling can be disregarded as possible coupling mechanisms. Additionally, as the temperature is lowered, the saturation magnetization, and therefore coupling via stray fields, would also be expected to be enhanced at reduced temperatures.

At room temperature, the overall shape of the major loop suggests that the $[Ni/Co]_2$ and $[Ni/Co]_5$ MLs are highly coupled, Fig. 2(b). Furthermore, the room-temperature FORC and MFM results, Figs. 3 and 4, not only confirm a highly coupled reversal but also that reversal proceeds by verti-

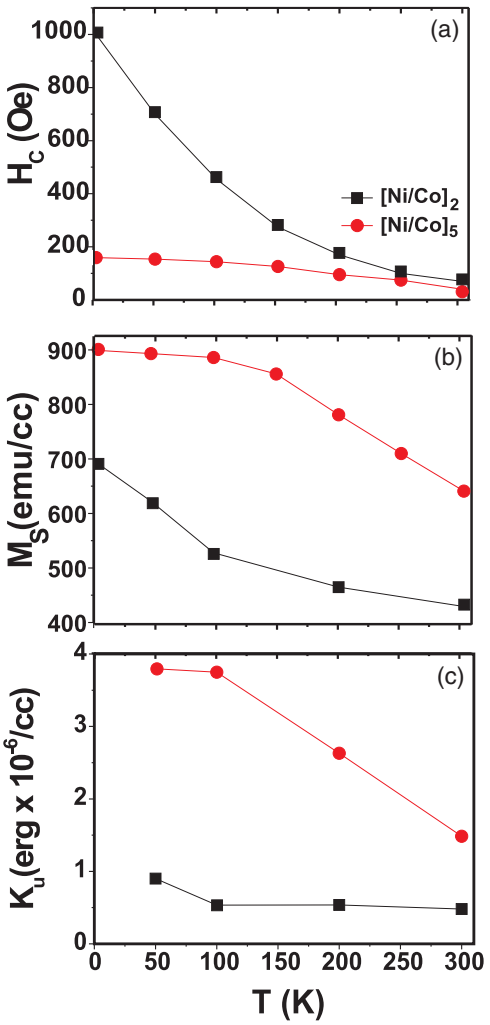

FIG. 6. (Color online) Temperature dependence of the (a) coercivity, (b) saturation magnetization, and (c) anisotropy constant for the isolated [Ni/Co]$_2$ (squares) [Ni/Co]$_5$ (circles) MLs.

cally correlated domains. Therefore the peaks in the major loop derivative, Fig. 2(b), should not be interpreted as the switching fields of the [Ni/Co]$_2$ and [Ni/Co]$_5$ MLs but as the nucleation and annihilation fields of reverse domains. Although the intrinsic domain size of the [Ni/Co]$_2$ and [Ni/Co]$_5$ MLs is different at room temperature, Figs. 4(a) and 4(b), the coercivity, Fig. 6(a), and anisotropy, Fig. 6(c), of each layer are also relatively small. This then allows for magnetostatically driven domain replication, evident in the reduced domain size of the PSV, Fig. 4(c). As the measurement temperature is reduced from 300 to 175 K, the reversal of the constituent ML remain locked and the nucleation (black squares) and annihilation fields (red circles) show a small and gradual increase, as expected for reduced temperatures, Fig. 7(c).

Reducing the measurement temperature below 175 K results in a complete decoupling of the [Ni/Co]$_2$ and [Ni/Co]$_5$ MLs, as evidenced in the distinct switching fields, Figs. 7(a) and 7(c), and rapid increase in MR, Figs. 7(b) and 7(d). Further evidence of this complete decoupling is found by measuring selected reversal curves at T = 50 K, Fig. 8. The two reversal

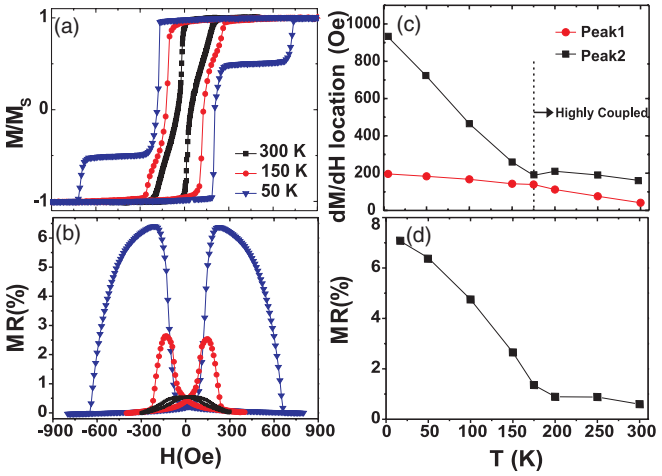

FIG. 7. (Color online) Hysteresis loops of the (a) magnetization and (b) magnetoresistance for the PSV with $t_{Cu} = 4.6$ nm measured at the indicated temperature. The temperature dependence of the major loop derivative peak locations and magnetoresistance are shown in (c) and (d), respectively.

curves, immediately after reversal of the [Ni/Co]$_5$ ML (red circles) and after partial reversal of the [Ni/Co]$_2$ ML (blue triangles), trace up along the same portion of the [Ni/Co]$_5$ ML minor loop. Therefore, the location of the derivative peaks, Fig. 7(c), which begin to significantly diverge for T < 175 K, should now be interpreted as the switching fields of the individual [Ni/Co]$_2$ and [Ni/Co]$_5$ MLs. In fact, the locations of the derivative peaks in Fig. 7(c) show good quantitative agreement with the coercivities of the isolated [Ni/Co]$_2$ and [Ni/Co]$_5$ MLs, Fig. 6(a), for T < 175 K.

The temperature dependence of this decoupling mechanism is rather straightforward. At elevated temperatures the coercivity and anisotropy of the constituent MLs are very similar. Therefore, the stray fields emanating from the [Ni/Co]$_5$ ML are able to initiate reversal domains in the [Ni/Co]$_2$ ML, thereby resulting in correlated reversal of both MLs. In essence the PSV is now behaving as a [Ni/Co]$_x$ ML with x = 7 bilayers, almost as if the Cu spacer was absent. However, at reduced temperatures the reversal properties of the constituent ML begin to diverge. The coercivity of the [Ni/Co]$_2$ ML increases

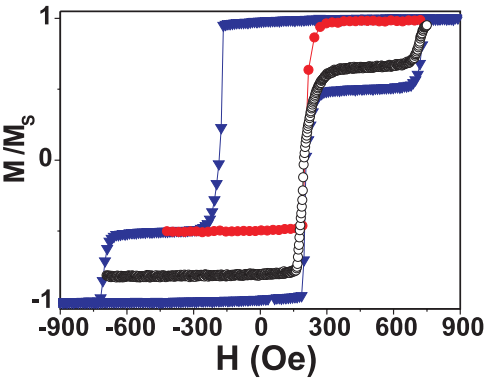

FIG. 8. (Color online) Major hysteresis loop with the applied field perpendicular to the film for the PSV with $t_{Cu} = 4.6$ nm measured at 50 K along with two reversal curves.

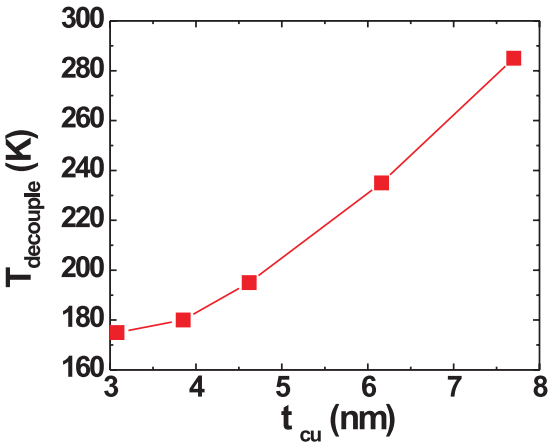

FIG. 9. (Color online) Dependence of the decoupling temperature, $T_{decouple}$, as a function of the spacer thickness, t_{Cu}.

to a point where the stray fields emanating from the $[Ni/Co]_5$ ML are no longer sufficient to initiate its reversal. Therefore the $[Ni/Co]_2$ and $[Ni/Co]_5$ MLs behave independently.

Finally, this coupling mechanism is probed as a function of spacer thickness in series of nominally identical PSVs. In Fig. 9, the temperature at which the $[Ni/Co]_2$ and $[Ni/Co]_5$ MLs begin to decouple, termed $T_{decouple}$, is plotted for $t_{Cu} \geqslant 3$ nm. Clearly, the temperature at which the MLs decouple strongly decreases as the spacer gets thinner. For thin spacer layers, where the dipolar interactions are stronger, it takes a lower temperature, and therefore a larger relative difference in ML coercivity, to break the dipolar coupling. We should also note that for $t_{Cu} < 3$ nm we were not able to observe any decoupling, even at our lowest possible measurement temperature of 1.8 K, which indicates the onset of another coupling mechanism.

V. CONCLUSION

The temperature-dependent coupling mechanisms in Ni/Co multilayer-based PSVs are investigated. Interestingly, for a relatively thick Cu spacer layer, the $[Ni/Co]_2$ and $[Ni/Co]_5$ MLs are completely coupled at room temperature. FORC and MFM measurements confirm that the reversal proceeds by vertically correlated domains through the entire film stack due to strong dipolar coupling through the Cu spacer leading to domain replication. Somewhat surprisingly, the MLs become completely decoupled when the measurement temperature is reduced, even though the saturation magnetization of the constituent MLs shows a strong increase. This decoupling is evident in both the switching properties and dramatic increase in MR. The dramatically different coercivities of the $[Ni/Co]_2$ and $[Ni/Co]_5$ MLs at reduced temperatures inhibits domain replication and therefore promotes decoupling. Finally, the decoupling temperature is found to increase with spacer thickness, further highlighting the critical role of dipolar interactions.

ACKNOWLEDGMENTS

Support from The Swedish Foundation for strategic Research (SSF) and The Swedish Research Council (VR) is gratefully acknowledged. Johan Åkerman is a Royal Swedish Academy of Sciences Research Fellow supported by a grant from the Knut and Alice Wallenberg Foundation.

*Corresponding author: majidm@kth.se

[1] G. Daalderop, P. Kelly, and F. den Broeder, Phys. Rev. Lett. **68**, 682 (1992).
[2] S. Mangin, D. Ravelosona, J. A. Katine, M. J. Carey, B. D. Terris, and E. E. Fullerton, Nat. Mater. **5**, 210 (2006).
[3] S. Mangin, Y. Henry, D. Ravelosona, J. A. Katine, and E. E. Fullerton, Appl. Phys. Lett. **94**, 012502 (2009).
[4] S. Girod, M. Gottwald, S. Andrieu, S. Mangin, J. McCord, E. E. Fullerton, J.-M. L. Beaujour, B. J. Krishnatreya, and A. D. Kent, Appl. Phys. Lett. **94**, 262504 (2009).
[5] W. H. Rippard, A. M. Deac, M. R. Pufall, J. M. Shaw, M. W. Keller, S. E. Russek, and C. Serpico, Phys. Rev. B **81**, 014426 (2010).
[6] T. Moriyama, T. J. Gudmundsen, P. Y. Huang, L. Liu, D. Muller, D. C. Ralph, and R. Buhrman, Appl. Phys. Lett. **97**, 072513 (2010).
[7] N. Funabashi, K. Aoshima, K. Machida, K. Kuga, T. Ishibashi, and N. Shimidzu, IEEE Trans. Magn. **46**, 1998 (2010).
[8] B. Dieny, R. C. Sousa, J. Herault, C. Papusoi, G. Prenat, U. Ebels, D. Houssameddine, B. Rodmacq, S. Auffret, L. D. B. Prejbeanu, M. C. Cyrille, B. Delaet, O. Redon, C. Ducruet, J P. Nozieres, and I. L. Prejbeanu, Int. J. Nanotechnol. **7**, 591 (2010).
[9] M. Carpentieri, G. Finocchio, B. Azzerboni, and L. Torres, Phys. Rev. B **82**, 094434 (2010).
[10] S. M. Mohseni, S. R. Sani, J. Persson, T. N. Anh Nguyen, S. Chung, Ye. Pogoryelov, and Johan Åkerman, Phys. Status Solidi RRL **5**, 432 (2011).
[11] Y. Zhou, C. L. Zha, S. Bonetti, J. Persson, and Johan Åkerman, Appl. Phys. Lett. **92**, 262508 (2008).
[12] C. L. Zha, J. Persson, S. Bonetti, Y. Y. Fang, and Johan Åkerman, Appl. Phys. Lett. **94**, 163108 (2009).
[13] Y. Zhou, S. Bonetti, C. L. Zha, and Johan Åkerman, New J. Phys. **11** 103028 (2009).
[14] C. L. Zha, R. K. Dumas, J. Persson, S. M. Mohseni, J. Nogués, and Johan Åkerman, IEEE Magn. Lett. **1**, 2500104 (2010).
[15] D. Houssameddine, U. Ebels, B. Delaet, B. Rodmacq, I. Firastrau, F. Ponthenier, M. Brunet, C. Thirion, J.-P. Michel, L. Prejbeanu-Buda, M.-C. Cyrille, O. Redon, and B. Dieny, Nat. Mater. **6**, 447 (2007).
[16] K. J. Lee, O. Redon, and B. Dieny, Appl. Phys. Lett. **86**, 022505 (2005).
[17] V. Baltz, S. Landis, B. Rodmacq, and B. Dieny, J. Magn. Magn. Mater. **290**, 1286 (2005).
[18] M. G. Samant and S. S. P. Parkin, Vacuum **74**, 705 (2004).
[19] M. Albrecht, G. Hu, A. Moser, O. Hellwig, and B. D. Terris, J. Appl. Phys. **97**, 103910 (2005).

[20]C. L. Zha, Y. Y. Fang, J. Nogues, and Johan Åkerman, J. Appl. Phys. **106**, 053909 (2009).
[21]L. Thomas, M. Samant, and S. Parkin, Phys. Rev. Lett. **84**, 1816 (2000).
[22]C. Cowache, B. Dieny, S. Auffret, M. Cartier, R. H. Taylor, R. O. Barr, and S. Y. Yamamoto, IEEE Trans. Magn. **34**, 843 (1998).
[23]W. Lew, S. Li, L. Lopez-Diaz, D. Hatton, and J. Bland, Phys. Rev. Lett. **90**, 217201 (2003).
[24]W. Kuch, L. Chelaru, K. Fukumoto, F. Porrati, F. Offi, M. Kotsugi, and J. Kirschner, Phys. Rev. B **67**, 214403 (2003).
[25]J. Wang, Y. Liu, P. P. Freitas, E. Snoeck, and J. L. Martins, J. Appl. Phys. **93**, 8367 (2003).
[26]J. M. Teixeira, J. Ventura, R. Fermento, J. P. Araujo, J. B. Sousa, S. Cardoso, and P. P. Freitas, J. Appl. Phys. **103**, 07F319 (2008).
[27]L. Néel, C. R. Acad. Sci. **255**, 1676 (1962).
[28]J. Moritz, F. Garcia, J. C. Toussaint, B. Dieny, and J. P. Nozieres, Europhys. Lett. **65**, 123 (2004).
[29]V. Baltz, A. Marty, B. Rodmacq, and B. Dieny, Phys. Rev. B **75**, 014406 (2007).
[30]Harrison W. Fuller and Donald L. Sullivan, J. Appl. Phys. **33**, 1063 (1962).
[31]B. Rodmacq, V. Baltz, and B. Dieny, Phys. Rev. B **73**, 092405 (2006).
[32]S. Wiebel, J.-P. Jamet, N. Vernier, A. Mougin, J. Ferre, V. Baltz, B. Rodmacq, and B. Dieny, Appl. Phys. Lett. **86**, 142502 (2005).
[33]T. Hauet, C. M. Günther, B. Pfau, M. E. Schabes, J. Thiele, R. L. Rick, P. Fischer, S. Eisebitt, and O. Hellwig, Phys. Rev. B **77**, 184421 (2008).
[34]J. Vogel, W. Kuch, R. Hertel, J. Camarero, K. Fukumoto, F. Romanens, S. Pizzini, M. Bonfim, F. Petroff, A. Fontaine, and J. Kirschner, Phys. Rev. B **72**, 220402 (2005).
[35]J. M. Shaw, H. T. Nembach, and T. J. Silva, J. Appl. Phys. **108**, 093922 (2010).
[36]R. K. Dumas, C. P. Li, I. V. Roshchin, I. K. Schuller, and Kai Liu, Phys. Rev. B **75**, 134405 (2007).
[37]J. E. Davies, O. Hellwig, E. E. Fullerton, and K. Liu, Phys. Rev. B **77**, 014421 (2008).
[38]J. E. Davies, O. Hellwig, E. E. Fullerton, G. Denbeaux, J. B. Kortright, and K. Liu, Phys. Rev. B **70**, 224434 (2004).
[39]S. Mangin, T. Hauet, P. Fischer, D. H. Kim, J. B. Kortright, K. Chesnel, E. Arenholz, and E. E. Fullerton, Phys. Rev. B **78**, 024424 (2008).
[40]C. Kittle, Phys. Rev. **70**, 965 (1946).
[41]O. Posth, C. Hassel, M. Spasova, G. Dumpich, J. Lindner, and S. Mangin, J. Appl. Phys. **106**, 023919 (2009).
[42]W. Sucksmith and J. E. Thompson, Proc. R. Soc. London, Ser. A **225**, 362 (1954).
[43]H. J. Richter, O. Hellwig, S. Florez, C. Brombacher, and M. Albrecht, J. Appl. Phys. **109**, 07B713 (2011).